Evaluation of protective shielding thickness for diagnostic radiology rooms: Theory and computer simulation

Paulo R. Costa[a)]
Instituto de Eletrotécnica e Energia, Universidade de São Paulo-Brasil, Av. Prof. Luciano Gualberto 1289, Cidade Universitária, 05508-900, São Paulo, SP, Brazil

Linda V. E. Caldas[b)]
Instituto de Pesquisas Energéticas e Nucleares, Comissão Nacional de Energia Nuclear, Travessa R, 400, Cidade Universitária, 05508-900, São Paulo, SP, Brazil

(Received 24 January 2001; accepted for publication 9 October 2001; published 26 December 2001)

This work presents the development and evaluation using modern techniques to calculate radiation protection barriers in clinical radiographic facilities. Our methodology uses realistic primary and scattered spectra. The primary spectra were computer simulated using a waveform generalization and a semiempirical model (the Tucker–Barnes–Chakraborty model). The scattered spectra were obtained from published data. An analytical function was used to produce attenuation curves from polycromatic radiation for specified kVp, waveform, and filtration. The results of this analytical function are given in ambient dose equivalent units. The attenuation curves were obtained by application of Archer's model to computer simulation data. The parameters for the best fit to the model using primary and secondary radiation data from different radiographic procedures were determined. They resulted in an optimized model for shielding calculation for any radiographic room. The shielding costs were about 50% lower than those calculated using the traditional method based on Report No. 49 of the National Council on Radiation Protection and Measurements.
 [DOI: 10.1118/1.1427309]

I. INTRODUCTION

The progression of using artificial sources of radiation is strongly related to the development of efficient methods for protecting workers and the public from the potential risks of these sources. These methods have been studied and improved since the earliest times of medical use of radiation. Archer[1] published a very clear description of the history of radiation shielding. This author described five historical periods since the last years of 19th century until the last decade as the main concepts of radiation protection were developed. Archer describes the development of radiation shielding methodology starting from the basic recommendations of Report No. 6 of the National Council on Radiation Protection and Measurements (NCRP),[2] and concluding with comments regarding the revision process of NCRP Report No. 49[3] (hereafter referred to as NCRP49).

NCRP49 presents methodologies to determine protective shielding for diagnostic and therapeutic x-ray rooms. It was written more than two decades ago and, in the case of diagnostic shielding, uses data obtained with x-ray technologies that are not in use anymore. Moreover, the NCRP49 formulation and data do not include information regarding mammography, computed tomography and digital radiography room shielding. Other limitations of this report include a lack of information regarding other shielding materials (besides lead and concrete), the conservatism of the "add one HVL" rule,[4] questions about limits for film storage, use and occupancy factors, and other design details.

Based on these arguments, the NCRP and the American Association of Physicists in Medicine (AAPM) constituted Task Group 9 with the aim of performing a revision for a new version of NCRP49. Since its creation, members of the Task Group 9 have published several papers[5–13] improving data and reviewing methods for shielding calculation for diagnostic rooms.

This work presents contributions for this new shielding evaluation method, taking into account the primary and scattered radiation energy distributions, as well as workload spectra[5,14] for diagnostic imaging modalities. The main object of the investigation was the development of a method for determining the thickness of a given material required to provide the proper attenuation for primary, scattered and leakage radiation spectra that reach a structural barrier in a radiological room. This methodology was combined with new information regarding spectral distributions of radiation scattered by a phantom in order to allow the determination of ambient dose equivalents in x-ray rooms. The product of this work consists of a model that provides a more accurate treatment for the problem of determining shielding thickness of barriers necessary for radiological room protection. The present work is a contribution for the search of a cost-effective formulation for diagnostic x-ray shielding.

II. METHODOLOGY

The present work proposes the generalization of formulations proposed by Dixon and Simpkin[9] for primary barriers and Simpkin and Dixon[12] for secondary barriers. This generalization consists in taking into account primary and secondary radiation spectra modulated by realistic workload distributions and evaluated in ambient dose equivalent units. To carry out these considerations, first a semiempirical model for evaluation of diagnostic spectra was modified in order to allow the calculation of radiation spectra considering different high voltage ripples. Second, these semiempirical spectra were calibrated considering experimental data relating air-kerma per mA min for different voltages and ripples. After these two steps, these calibrated x-ray spectra were compared to experimental data. Finally, these spectra were used on the generalization of previous works.[10,11]

A. Waveform generalization of the semiempirical Tucker–Barnes–Chakraborty model

1. The original model

Tucker *et al.*[15] introduced a model [the Tucker–Barnes–Chakraborty (TBC) model] which proposed two different formulations for evaluating the radiation spectra emitted by an x-ray tube. These formulations take into account the continuous (*bremsstrahlung*) spectra and the characteristic emission. The TBC model considers the target material, the tube design, and the composition of materials that attenuate the radiation beam before emerging from the tube housing. The equation adopted for the *bremsstrahlung* contribution is

$$N^B(E)dE=\frac{\sigma_0 Z^2}{A}\frac{dE}{E}\int_E^{T_0}\frac{B(E,T)}{T}F(E,T,\theta)\left(\frac{1}{\rho}\frac{dT}{dx}\right)^{-1}dT, \tag{1}$$

where $\sigma_0=\alpha r_e^2$, with α as the fine structure constant and r_e the classical radius of the electron. Z is the effective atomic number of the target material, A is the atomic mass of the target atoms, T_0 is the kinetic energy of the electrons when they reach the target, T is the kinetic energy of electrons inside the target at a distance x from the surface, and E is the energy of the photons produced by the electrons. The expression $(1/\rho)(dT/dx)$ represents the mass stopping power of the target material, $B(E,T)$ is a function proportional to the number of photons produced by each incident electron, and $F(E,T,\theta)$ represents the filtration provided by the anode layer and materials between the target and the measuring point (tube glass, oil, plastics, air). In this function, θ represents the anode angle.

The TBC model proposed the function $J(x/R)$ to represent the probability for characteristic emission. This probability was modeled as a parabolic function that drops to zero when the electron energy is equal to the k-edge binding energy, E_k, or

$$J(x/R)=\begin{cases}\left(\frac{3}{2}\right)\left[1-\left(\frac{x}{R}\right)^2\right] & \text{for } x\leqslant R\\ 0 & \text{for } x>R\end{cases}, \tag{2}$$

where R is the distance inside the target where the average kinetic energy of the electrons is equal to E_k. Therefore, the characteristic radiation production can be modeled as

$$N^c(E_i)=A_k\left(\frac{T_0}{E_k}-1\right)^{n_k}f(E_i)\int_0^R J\left(\frac{x}{R}\right)\times\exp[-\mu_w(E_i)x/\sin\theta]dx. \tag{3}$$

A_k and n_k are model parameters obtained by using a nonlinear least-squares method and $f(E_i)$ is the fractional x-ray characteristic emission of photons with energy E_i. The parameter A_k represents the number of characteristic photons emitted by incident electrons. Moreover, the distance R can be calculated as $R=(T_0^2-E_k^2)/\rho C(T_0)$ where $C(T)$ is the Thomson–Whiddington constant. In the present work, Birch and Marshall[16] data for this constant were fitted by a linear function using a least-squares method.

2. Waveform generalized model

The TBC waveform generalized model can be determined taking into account the applied voltage waveform represented by

$$V(t)=\frac{1}{f}\sum_{j=1}^{f}V_{\max}\left|\sin\left[\pi\left(12\times10^{-3}t-\frac{j-1}{f}\right)\right]\right|. \tag{4}$$

In Eq. (4), $V_{\max}$ is the peak potential in kV units, t is the time interval during the exposure in milliseconds, and f is a parameter representative of the frequency of the high voltage generator.

Equations (1)–(4) provide the basis for the waveform generalized model. This approach considers the high voltage applied to the tube as a function of the exposure time and calculates a series of elemental TBC spectra for each time interval. Considering a waveform $V(t)$ that produces a ripple ϕ, this formulation can be synthesized by

$$N_p^{\phi}(E)=\int_0^{t_{\exp}}N(E,V(t))dt, \tag{5}$$

where $t_{\exp}$ is the exposure time selected in the x-ray machine. A similar formulation was published by Kramer *et al.*[17]

3. Calibration in SI units

For the purpose of the developed model, the x-ray spectra can be calibrated in dosimetric units. This calibration must be related to functional parameters of the x-ray machine in order to be useful to the present work. To perform this calibration, the definition of the quantity air-kerma[18] normalized by the tube workload (mGy/mA min) can be used and it is given by

$$D^{\phi}(V)=C^{\phi}(V)\int_0^V N_p^{\phi}(E)\left(\frac{\mu(E)}{\rho}\right)_{\text{air}}E_{\text{tr}}^m(E)dE. \tag{6}$$

In Eq. (6) the function $C^{\phi}(V)$ provides the normalization of the radiation spectra in units of mGy/mA min. Moreover, $(\mu(E)/\rho)_{\text{air}}$ represents the mass attenuation coefficient for the air, and E_{tr}^m is the mean energy transferred to electrons of the medium. Dixon and Simpkin[9] proposed the use of a simple power law to represent the relationship between air-kerma per mAs and applied voltage for the diagnostic range. Using the proposed equation, the function $C^{\phi}(V)$ can be calculated as

$$C^{\phi}(V)=\frac{A^{\phi}V^{B^{\phi}}}{\int_0^V N_p^{\phi}(E)\left(\frac{\mu(E)}{\rho}\right)_{\text{ar}}E_{\text{tr}}^m(E)dE}. \tag{7}$$

TABLE I. A^{ϕ} and B^{ϕ} values for different waveforms calculated from experimental measurements performed by Archer *et al.* (Ref. 5) for full-wave single-phase and twelve-pulse three-phase equipment and by Tucker *et al.* (Ref. 15) for a constant potential system.

Waveform	Constant A^{ϕ} [μGy/mA s]	B^{ϕ}
Full-wave single-phase	5.30×10^{-4}	1.904
Twelve-pulse three-phase	7.30×10^{-4}	1.898
Constant potential	2.12×10^{-3}	1.679

Table I shows the results for parameters A^{ϕ} and B^{ϕ} for different waveforms. Using Eqs. (5) and (7), the calibrated x-ray spectra can be evaluated by

$$N_{p,n}^{\phi,V}(E)=C^{\phi}(V)\,N_{p}^{\phi}(E). \tag{8}$$

In Eq. (8), the indexes ϕ and V represent the waveform ripple and the applied voltage, respectively. p denotes modeling of the primary beam and n that the resulting spectra is normalized in units of air-kerma per mA s. Similar equations can be used for calculating radiation spectra generated by mammographic equipment. In this case, the equations adopt calculation parameters presented by Tucker *et al.*[19] Table II shows the results of the integration of the calculated spectra using Eq. (8). These results were compared to the data published by Tucker[15] and calculated by using a formulation presented in Wolbarst.[20]

4. Experimental verification

An experimental verification of the spectra provided by the application of Eqs. (1) and (3) was carried out by comparison of computer simulations of this formulation, performed by using a Mathcad (Mathsoft, Inc.) worksheet, with experimental measurements performed by using a *PIN* photodiode operating at room temperature. The experimental methodology and instrumentation was presented by Terini *et al.*[21] The energy resolution of the photodiode measurements was about 3 keV. Experimental measurements performed by Fewell[22] at the Center for Devices and Radiological Health/US-Food and Drug Administration laboratories were also used. The radiation spectra measured by Fewell using a Ge detector were standardized considering the IEC 1267[23] and NIST[24] high voltage and HVL set-up conditions. Figures 1 and 2 present comparisons of the TBC waveform generalized model and experimental results from Terini *et al.*[21] Table III shows the experimental conditions used for this comparison. The x-ray equipment was composed of a Siemens Heliophos 4B HV transformer coupled to a 150/30/50 Rörix x-ray tube. The system was operated in fluoroscopic mode in these measurements. The computer-simulated spectra used the same parameters to evaluate the generalized semiempirical spectra showed as continuous lines in the Figs. 1 and 2. Figures 3 and 4 show comparisons using data obtained by Fewell[22] and Table IV presents the experimental conditions used. Other comparative results using different waveform conditions are shown in Ref. 25.

In order to assure that the formulation used to generate the x-ray spectra is adequate to represent attenuation curves, a

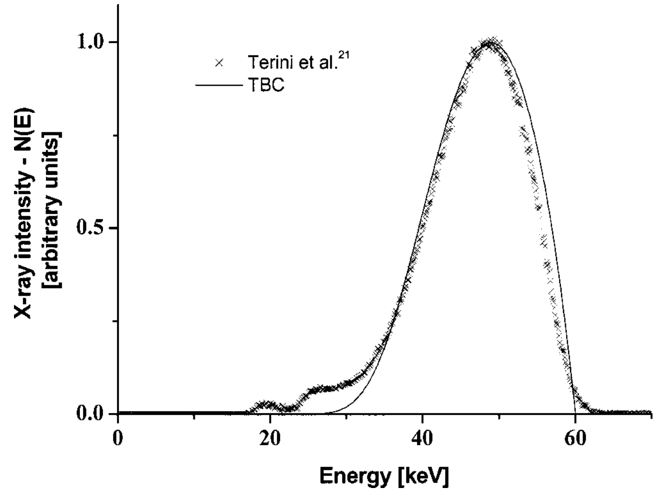

FIG. 1. Comparative results between measurements performed by a Si photodiode operated at room temperature (Ref. 21) and computer simulation using the waveform generalized TBC model. The experimental conditions are presented in Table III for high voltage of 60 kVp, and were the same used for the computer simulation.

TABLE II. Results for air-kerma per mA s at 1 m from the focal spot measured by Tucker *et al.* (Ref. 15) and calculated using the formula presented by Wolbarst (Ref. 20). These values are comparable to results obtained by integrating Eq. (8) of the present work. Different applied voltages, ripples of 0%, 0.83%, 3.41% and 100%, and a total filtration of 3 mm Al were considered.

Voltage (kVp)	TBC (μGy/mA s at 1 m) 0%	Wolbarst (μGy/mA s at 1 m) 3.41%	Wolbarst 100%	Present work (μGy/mA s at 1 m) 0.83%	Present work 3.41%	Present work 100%
70	42.7	42.11	25.26	44.23	38.68	28.84
80	54.8	55.00	33.00	55.35	49.84	37.19
90	67.9	69.61	41.77	67.45	62.33	46.54
100	81.1	85.94	51.56	80.50	76.13	56.88
110	95.3	103.98	62.38	94.47	91.23	68.20
120	109.9	123.75	74.25	109.32	107.62	80.49
130	124.9	145.23	87.13	125.05	125.27	93.74
140	140.9	168.44	101.06	141.61	144.20	107.95

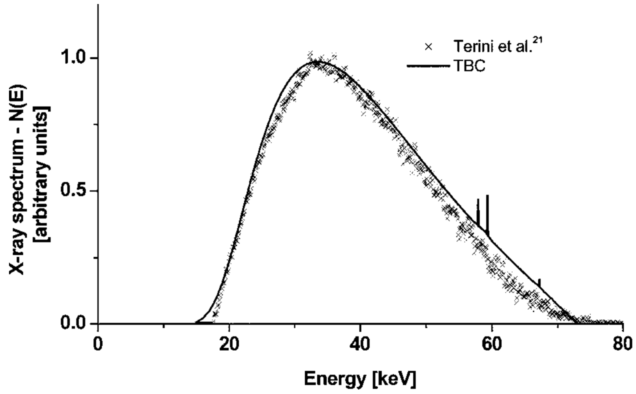

FIG. 2. Comparative results between measurements performed by a Si photodiode operated at room temperature (Ref. 21) and computer simulation using the waveform generalized TBC model. The experimental conditions are presented in Table III for high voltage of 73 kVp, and were the same used for the computer simulation.

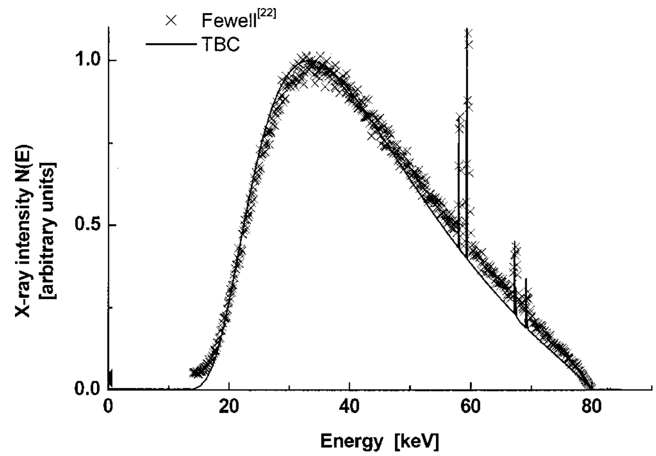

FIG. 3. Comparative results between Ge detector measurements (Ref. 22) and computer simulation using the waveform generalized TBC model. The experimental conditions are presented in Table IV for high voltage of 80 kVp, and were the same used for the computer simulation.

comparison was performed by using attenuation data from these generated spectra and experimental attenuation data from Ref. 26. Results from this comparative study are presented in Fig. 5. The solid curve presented in Fig. 5 refers to the integration in energy of the generated spectra multiplied by a factor $e^{-\mu(E)x}$ In this calculation, values of $\mu(E)$ for lead were used and x represents thickness of lead ranging from 0 to 2.3 mm. The resulting curve was normalized to be plotted together the data from Ref. 26. The small differences between experimental and computer-generated attenuation data appear because of differences in their values for the first and second HVL. By this result, the developed generalized method for generating x-ray spectra was considered adequate to be used to generate the attenuation curves for the optimized model for shielding barriers.

5. Scattered spectra

The TBC model provides a formulation for computing only primary spectra generated by conventional or mammographic systems. However, scattered spectra in simulated diagnostic conditions have been studied and measured by several authors.[27–31] In order to implement the generalized equations for shielding scattered radiation, a group of spectra measured by Fehrenbacher *et al.*[30,31] was used. These spectra were scattered by a perspex wall water phantom with dimensions of $30\times30\times15\,\text{cm}^3$. The measurements were taken in angles of 10°, 45°, 90°, 135°, and 142° in relation to the primary beam, using voltages of 52, 60, 70, 80, 90, 100 and 110 kVp. The beam area was $16\times16\,\text{cm}^2$ at the phantom surface. Therefore, these authors covered all the conventional diagnostic range of voltage and the most important scattered beam directions. For mammography calculations, the data published by Simpkin[32] and Simpkin and Dixon[12] were used. Figure 6 shows the scattered spectra measured in different angles at 100 kVp and Fig. 7 shows the scattered spectra at 90° for different applied voltages.

TABLE III. Experimental conditions used during measurements of spectra presented in Figs. 1 and 2.

Voltage (kVp)	Current (mA)	Additional filtration (mm Al)	(mm Cu)	Ripple (%)
60	~2	3.4	0.6	~2
73	~2	1.2	0	~2

B. Optimized model for shielding barriers calculation

1. Primary radiation

The concept of workload spectra (or distribution) was introduced by Simpkin[6,14] and it was extensively used in the present formulation. The use of radiation spectra associated with this concept was previously proposed by Costa and Caldas.[33–36] The formulation considers $S_0^p(E)$ as the radiation distribution reaching a primary barrier located at a distance d_p from the focal spot, weighted by the workload distribution, $w(v)$, as

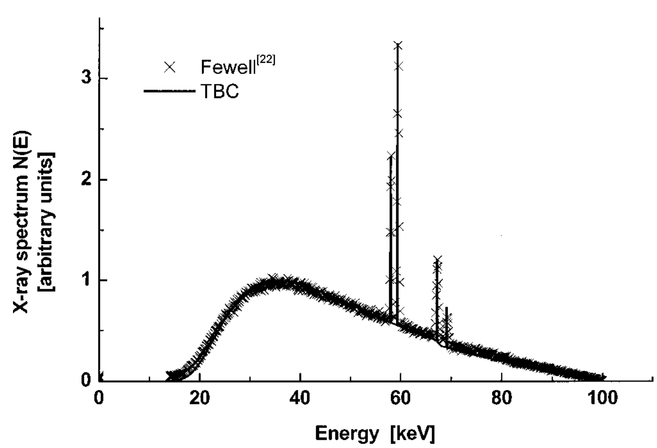

FIG. 4. Comparative results between Ge detector measurements (Ref. 22) and computer simulation using the waveform generalized TBC model. The experimental conditions are presented in Table IV for high voltage of 100 kVp, and were the same used for the computer simulation.

TABLE IV. Experimental conditions used by Fewell (Ref. 22) for obtaining the radiation spectra following IEC (IEC80)—Ref. 23 and NIST (M100)—Ref. 24 standards which are presented in Figs. 3 and 4. The corresponding TBC generated spectra used the same voltage parameters, and inherent and added filtration choice in order to provide equivalent first and second half-value layers.

Beam	Voltage (kVp)	HVL by Fewell (mm Al)		HVL by computer simulation (mm Al)		Total filtration used by Fewell (mm Al)	Total filtration adopted for calculation (mm Al)
		First HVL	Second HVL	First HVL	Second HVL		
IEC80	80	2.59	6.52	2.59	6.42	2.48	2.84
M100	100	4.89	11.61	4.89	11.42	5.26	6.25

$$S_0^p(E)=\frac{1}{d_p^2}\sum_V N_{p,n}^{\phi,V}(E)W(V). \quad (9)$$

According to the previously defined radiation spectra and the definition of workload spectra,[6,14] Eq. (9) provides the weighted primary spectrum in units of air-kerma per keV. However, current radiation protection standards[37] propose the use of the quantity ambient dose equivalent in order to quantify the efficiency of a given radiation shielding. Therefore, the present work introduces the following function to represent primary radiation levels in terms of ambient dose equivalent at a distance of 1 m of the focal spot:

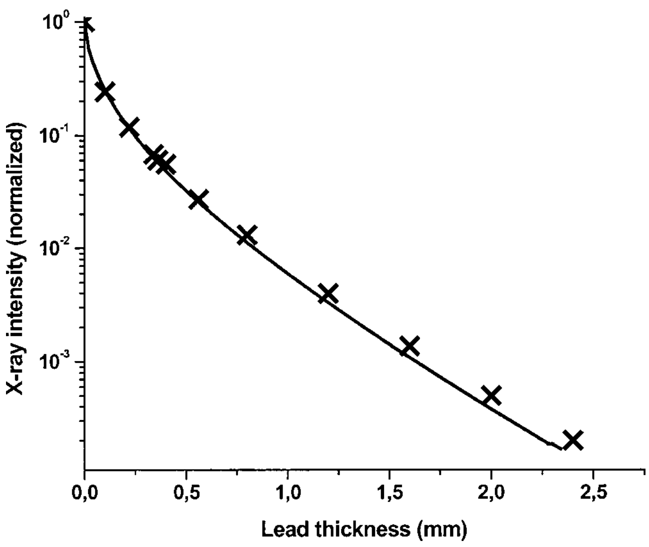

FIG. 5. Comparative results between an attenuation curve from x-ray generated spectrum (solid curve) and experimental data from Ref. 26 (X's). The semiempirical spectrum was generated using 100 kVp, considering a three-phase generator and an x-ray tube with target angle of 12.5° and inherent filtration of 0.5 mm Al. An additional filtration of 2.35 mm Al was also considered. The first and second HVL of these spectra where calculated as 3.49 mm Al and 8.47 mm Al, respectively. The experimental data were obtained by using similar conditions, and the first and second HVL were tabulated in Ref. 26 as 3.46 mm Al and 8.8 mm Al. The solid curve refers to the integration in energy of the generated spectra multiplied by a factor $e^{-\mu(E)x}$. In this calculation, we used values of $\mu(E)$ for lead and x represents thickness of lead ranging from 0 to 2.3 mm. The resulting curve was normalized to be plotted together with the data from Ref. 26.

$$H_p^{m,\phi}(10,x_p)=\sum_V \int_0^V\left(\frac{H^*(10)}{K_{\text{ar}}}\right)\times(E)N_{p,n}^{\phi,V}(E)W(V)e^{-\mu_m(E)x_p}dE. \quad (10)$$

The function $(H^*(10)/k_{\text{ar}})(E)$ provides the unit conversion from air-kerma units (gray) to ambient dose equivalent (sievert).[37,38] In this function, the number 10 represents the depth, in millimeters, inside the ICRU sphere, where the ambient dose equivalent is evaluated. Figure 8 shows the representation of this function for the diagnostic energy range. The strong energy dependence of this function in this range is the main argument to the most accurate correction proposed in Eq. (10). Moreover, the function $\mu_m(E)$ represents the linear attenuation coefficient of the protective material and x_p is the thickness of the protective material used to shield the primary beam. In addition, Archer's model[4,5] can advantageously be used to rewrite Eq. (10) as

$$H_p^{m,\phi}(10,x_p)=H_p^{0,\phi}(10)\left[\left(1+\frac{\beta_p^m}{\alpha_p^m}\right)e^{\alpha_p^m\gamma_p^m x_p}-\frac{\beta_p^m}{\alpha_p^m}\right]^{1/\gamma_p^m}, \quad (11)$$

where α_p^m, β_p^m and γ_p^m are fitting parameters obtained by

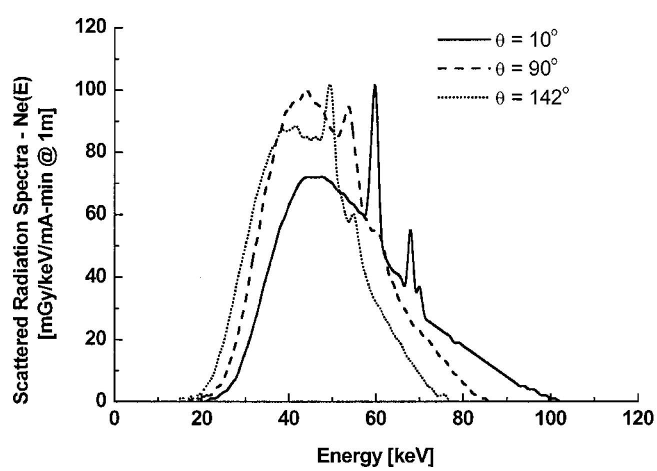

FIG. 6. Scattered radiation spectra measured by Fehrenbacher *et al.* (Ref. 30) related to a 100 kVp primary beam at scattering angles of 10°, 90°, and 142°. The primary beam was scattered by a $30\times30\times15\ \text{cm}^3$ water phantom with Perspex walls.

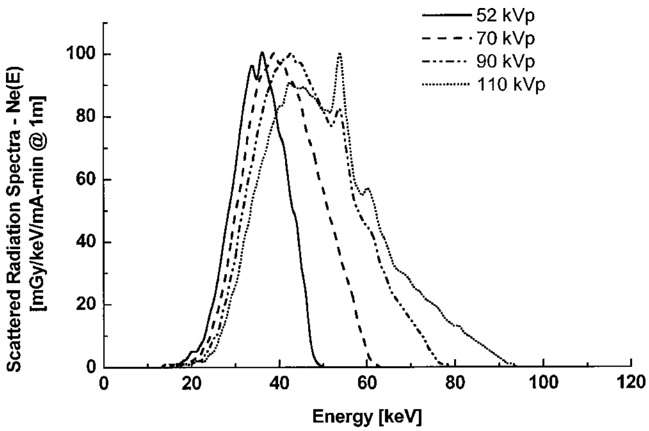

FIG. 7. Scattered radiation spectra measured by Fehrenbacher *et al.* (Ref. 30) related to a 90° scattering angle and corresponding to primary beams generated by potentials of 52, 70, 90, and 110 kVp. The primary beam was scattered by a $30\times 30\times 15\,\mathrm{cm}^3$ water phantom with Perspex walls.

applying a nonlinear least-squares method to data calculated from Eq. (10), x_p is the thickness of primary beam protective material, and

$$H_p^{0,\phi}(10)=\sum_V \int_0^V \left(\frac{H^*(10)}{K_{\mathrm{ar}}}\right)(E)N_{p,n}^{\phi,V}(E)W(V)dE. \quad (12)$$

Equation (12) represents the ambient dose equivalent at 1 m from the focal spot with no protective material.

2. Scattered radiation

Simpkin and Dixon[12] revised scatter-to-primary ratio data from Trout and Kelley[39] presented in NCRP49. According to these authors, the scattered radiation must take into account the scatter-to-primary ratio as a function of the scattering angle and the applied voltage. In the present work this ratio was calculated as

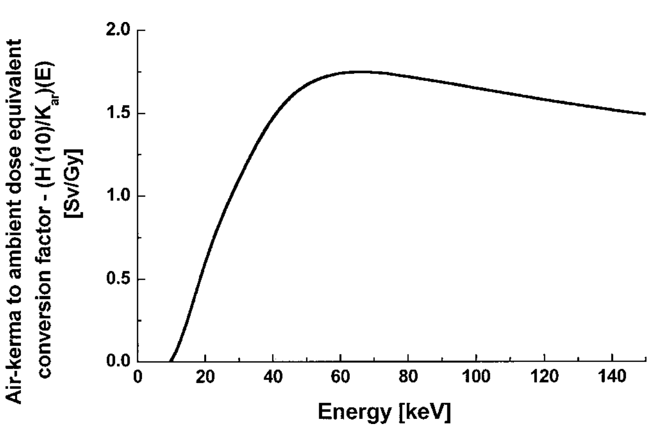

FIG. 8. Air-kerma to ambient dose equivalent conversion factor as a function of energy in the diagnostic range. The function corresponds to 10 mm in depth of the ICRU sphere $(H^*(10))$. The values were obtained from Refs. 37 and 38.

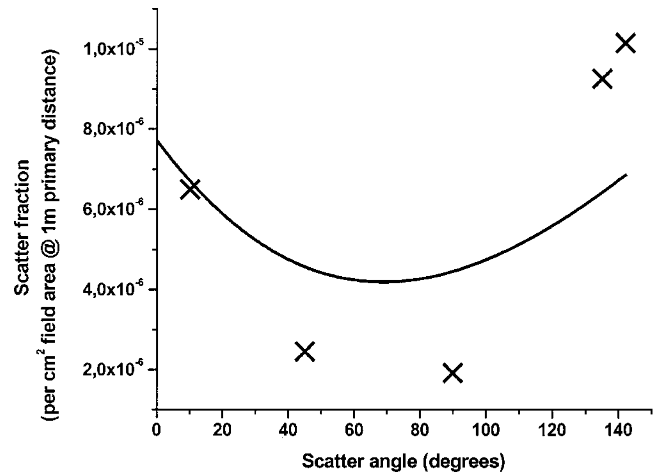

FIG. 9. Comparative results from data obtained by application of Eq. (13) (X's) and a polynomial fit proposed by Simpkin and Dixon (Ref. 12) (solid curve). This comparison shows that data used to simulate the scatter fraction [Eq. (13)] produces similar values for angles near the incident direction, lower values for angles around 90° (lateral scattering) and higher values for angles around 140° (backscattering), when compared to the model proposed by Simpkin and Dixon (Ref. 12). These differences are probably due to the different geometrical setup used by Fehrenbacher *et al.* (Ref. 30), adopted in the present work, and that by Trout and Kelley, adopted for obtaining the fitting curve by Simpkin and Dixon (Ref. 12).

$$a'(V,\theta)=\frac{10^6}{F'}\,\frac{\int_0^{E_{\max}}\left(\frac{H^*(10)}{K_{\mathrm{ar}}}\right)(E)N_e^{\phi,V}(E,\theta)W(V)dE}{\int_0^{E_{\max}}\left(\frac{H^*(10)}{K_{\mathrm{ar}}}\right)(E)N_p^{\phi,V}(E)W(V)dE}. \quad (13)$$

$N_e^{\phi,V}(E)$ is the scattered spectra at 1 m from the center of the scattering material considering an incident spectrum $N_p^{\phi,V}(E)$ produced by exciting an x-ray tube with a voltage V and ripple ϕ. The model considers the incident beam reaching the scattering object at an area F' when the focal spot to scatter medium distance is d'.

This formulation was compared to a polynomial fit proposed by Simpkin and Dixon.[12] An example of this comparison is presented in Fig. 9 where results are presented from the application of Eq. (13) for angles of 10°, 45°, 90°, 135°, and 142° by using spectral data from Ref. 30 and the polynomial fit. Figure 9 shows that the data used to simulate the scatter fraction [Eq. (13)] produces similar values for angles near the incident direction, lower values for angles around 90° (lateral scattering), and higher values for angles around 140° (backscattering), when compared to the model proposed by Simpkin and Dixon.[12] These differences are probably due to the different geometrical setup used by Fehrenbacher *et al.*,[30] adopted in the present work, and that by Trout and Kelley, adopted for obtaining the fitting curve by Simpkin and Dixon.[12] Despite these differences, the proposed equation was considered adequate for the calculation of scatter fractions for the purpose of the present work, since the behavior of both models is similar.

Using the scatter-to-primary ratio defined in Eq. (13), the ambient dose equivalent resulting from the scattered radia-

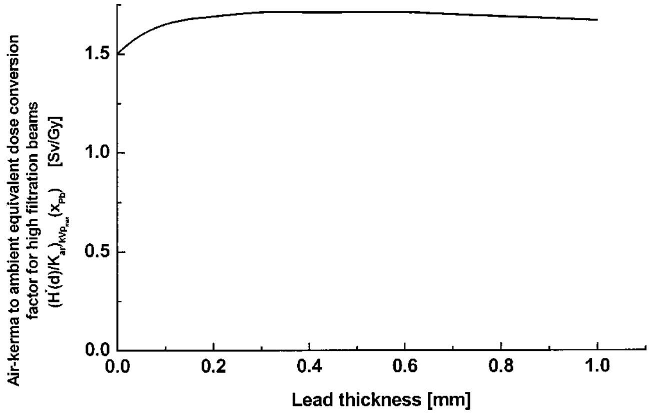

FIG. 10. Air-kerma to ambient dose equivalent conversion factor for high filtration beams as a function of the lead thickness. The measurements were performed by Peixoto (Ref. 41) by using a 150 kVp x-ray beam (4 mm Al HVL).

tion produced by a workload spectra which reaches a scattering medium distant d_F from the focal spot, corresponding to an area[12] $F=[F'\times(d_F/d')^2]$, can be defined as

$$H_{e,\theta}^{m,\phi}(10,x_e)=\sum_V a'(V,\theta)\times 10^{-6}\frac{F}{d_F^2}\int_0^V\left(\frac{H^*(10)}{K_{\mathrm{ar}}}\right)\times(E)N_e^{\phi,V}(E,\theta)W(V)e^{-\mu_m(E)x_e}dE, \quad (14)$$

where x_e is the thickness of shielding material used as protection for the scattered radiation. As in the case of primary radiation, Eq. (14) can be written as

$$H_{e,\theta}^{m,\theta}(10,x_e)=H_{e,\theta}^{0,\phi}(10)\left[\left(1+\frac{\beta_e^m}{\alpha_e^m}\right)e^{\alpha_e^m\gamma_e^m x_e}-\frac{\beta_e^m}{\alpha_e^m}\right]^{-1/\gamma_e^m}, \quad (15)$$

where α_e^m β_e^m and γ_e^m are fitting parameters obtained by using a nonlinear least-squares method to data calculated from Eq. (14), x_e is the thickness of the scattered beam protective material, and

$$H_{e,\theta}^{0,\phi}(10)=\sum_V a'(V,\theta)\times 10^{-6}\frac{F}{d_F^2}\int_0^V\left(\frac{H^*(10)}{K_{\mathrm{ar}}}\right)\times(E)N_e^{\phi,V}(E,\theta)W(V)dE. \quad (16)$$

3. Leakage radiation

Using the model of Simpkin and Dixon,[12] if L is the air-kerma rate measured at 1 m from the focal spot when the x-ray tube is excited using the nominal x-ray tube voltage under conditions of loading corresponding to the maximum specified energy input in 1 h,[40] then the lead thickness needed to obtain this level of protection can be evaluated by

$$L=I_{\max}\times 60\int_0^{V_{\max}}N_p^{\phi,V_{\max}}(E)e^{-\mu_{\mathrm{Pb}}(E)x_e}dE. \quad (17)$$

In this equation, $I_{\max}$ is the maximum continuous anode current, in mA, for the safe operation of the tube at its maximum voltage $V_{\max}$, $\mu_{\mathrm{Pb}}(E)$ is the linear attenuation coefficient of lead, and x_c is the lead thickness needed to reduce the leakage radiation to L.

Therefore, the leakage radiation from an x-ray tube housing when the equipment is operated following a workload distribution $W(V)$ can be evaluated by

$$H_f^{0,\phi}(10)=L\left(\frac{H^*(10)}{K_{\mathrm{ar}}}\right)_{V_{\max}}^{\mu_{\mathrm{Pb}}}\frac{\sum_V\int_0^V\left(\frac{H^*(10)}{K_{\mathrm{ar}}}\right)(E)N_{p,n}^{\phi,V}(E)W(V)e^{-\mu_{\mathrm{Pb}}(E)x_c}dE}{I_{\max}\times 60\int_0^{V_{\max}}\left(\frac{H^*(10)}{K_{\mathrm{ar}}}\right)(E)N_{p,n}^{\phi,V_{\max}}(E)e^{-\mu_{\mathrm{Pb}}(E)x_c}dE}. \quad (18)$$

The parameter $(H^*(10)/K_{\mathrm{ar}})_{v_{\max}}^{x_{\mathrm{Pb}}}$ is the air-kerma to ambient dose equivalent conversion factor considering high filtration beams.[41] In Fig. 10 a plot of this conversion factor as a function of lead thickness is presented.

Therefore, the ambient dose equivalent from leakage radiation after a shielding barrier of thickness x_f can be calculated as

$$H_f^{m,\phi}(10,x_f)=L\left(\frac{H^*(10)}{K_{\mathrm{ar}}}\right)_{V_{\max}}^{\mu_{\mathrm{Pb}}}\frac{\sum_V\int_0^V\left(\frac{H^*(10)}{K_{\mathrm{ar}}}\right)(E)N_{p,n}^{\phi,V}(E)W(V)e^{-\mu_{\mathrm{Pb}}(E)x_c}e^{-\mu_m(E)x_f}dE}{I_{\max}\times 60\int_0^{V_{\max}}\left(\frac{H^*(10)}{K_{\mathrm{ar}}}\right)(E)N_{p,n}^{\phi,V_{\max}}(E)e^{-\mu_{\mathrm{Pb}}(E)x_c}dE}. \quad (19)$$

Following the previous examples, Eq. (19) can be written by using Archer's model[4,5] as

$$H_f^{m,\phi}(10,x_f)=H_f^{0,\phi}(10)\left[\left(1+\frac{\beta_f^m}{\alpha_f^m}\right)e^{\alpha_f^m\gamma_f^m x_f}-\frac{\beta_f^m}{\alpha_f^m}\right]^{-1/\gamma_f^m}. \quad (20)$$

4. Total secondary radiation

It is more convenient for shielding barrier calculation to consider the secondary radiation instead of scattered and leakage radiations separately. Therefore, Eqs. (15) and (20) can be combined to produce

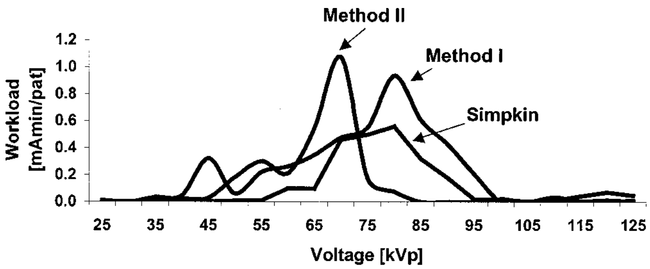

FIG. 11. Workload spectra obtained in the present work by methods I and II, and published by Simpkin (Ref. 6) for general radiography technique.

$$H_{s,\theta}^{m,\phi}(10,x_s)=\frac{H_{e,\theta}^{m,\phi}(10,x_s)}{d_e^2}+\frac{H_f^{m,\phi}(10,x_s)}{d_f^2}$$

$$=H_{s,0}^{0,\phi}\left[\left(1+\frac{\beta_s^m}{\alpha_s^m}\right)e^{\alpha_s^m\gamma_s^m x_s}-\frac{\beta_s^m}{\alpha_s^m}\right]^{-1/\gamma_s^m}, \qquad (21)$$

where

$$H_{s,\theta}^{0,\phi}=\frac{H_{e,\theta}^{m,\phi}(10)}{d_e^2}+\frac{H_f^{m,\phi}(10)}{d_f^2}. \qquad (22)$$

5. General solution for diagnostic shielding barriers

Equations (11), (15), and (20) are functional representations of primary, scattered, and leakage radiations typically found in diagnostic x-ray rooms. These equations are dependent on the constants, α, β, and γ, which are obtained by applying Archer's model[4,5] for the used shielding material. This model is especially useful in order to obtain workload-related curves calibrated in ambient dose equivalent units, which can be directly used for the shielding purpose. The function $W(V)$ represents the workload spectrum[6,14] for the considered diagnostic modality and charge of use for the x-ray equipment.

Therefore, a generic shielding barrier can be obtained using the following inequality:

$$\frac{H_p^{m,\phi}(10,x_t^m)}{d_p^2}U+\left[\frac{H_{e,\theta}^{m,\phi}(10,x_t^m)}{d_e^2}+\frac{H_f^{m,\phi}(10,x_t^m)}{d_f^2}\right](1-U)$$

$$\leqslant\frac{P}{T}, \qquad (23)$$

where U is the use factor, T is the occupational factor, and P is the dose level limit for the area to be protected. Solving this equation to x_t, the shielding thickness can be determined, providing the optimized radiation level in the room's neighborhood for a given workload spectrum.

III. APPLICATION

A. Workload spectra

A survey of workload spectra was carried out in 14 Brazilian imaging departments, which included general radiography, chest radiography, cardiac angiography, mammography, and computed tomography dedicated radiation rooms. Two different methods for data collection were used. Method I used data collected by observing the operational techniques applied in 605 examinations. The data corresponding to method II were obtained by interviewing 51 technicians; they were questioned about the most usual parameters selected for different examinations. The average results were compared to Simpkin[6] data (Fig. 11). Table V shows the comparative results for average weekly workload per patient for the evaluated diagnostic techniques. For comparison, in Table V data from Simpkin[6] and Archer[8] are also presented.

B. Attenuation curves

Figure 12 shows the attenuation curves for primary beams from general radiography, chest, and cardiac angiography techniques obtained by applying Eq. (11). For the general radiography technique, the workload spectra utilized corresponds to the method II described, supposing the use of constant potential x-ray equipment. The curves for chest technique also correspond to workload spectra obtained by

TABLE V. Average workload results for different radiological rooms. The columns "Other authors" show results extracted from Ref. 6 for general radiography, chest, mammography, and cardiac angiography and from Ref. 11 for computed tomography. The column "Present work" shows results obtained by method I (upper line) and by method II (lower line), or only by method II. The indications ND refer to nondetermined information.

	Workload per patient (mA min patient^{-1})		Patients per week		Total workload (mA min week^{-1})	
Diagnostic room	Other authors	Present work	Other authors	Present work	Other authors	Present work
General	2.45±0.09	4.55±1.28	112± 34	196± 14	274± 84	890± 111
radiography		2.68±0.30		346± 12		928± 107
Chest	0.22±0.01	0.23±0.06	206±103	181± 14	44± 22	41± 11
Mammography	6.69±0.14	4.3± 1.5	47.4± 5.3	118.0± 6.4	317± 36	504± 178
		4.3± 1.5		41.2± 1.8		400± 41
Cardiac	160± 11	183± ND	19.1± 3.7	25±ND	3050±628	4575± MD
amgopgraphy						
Computed	205± ND	288± 95	64±ND	44.5± 1.9	13 000±ND	12 800±4261

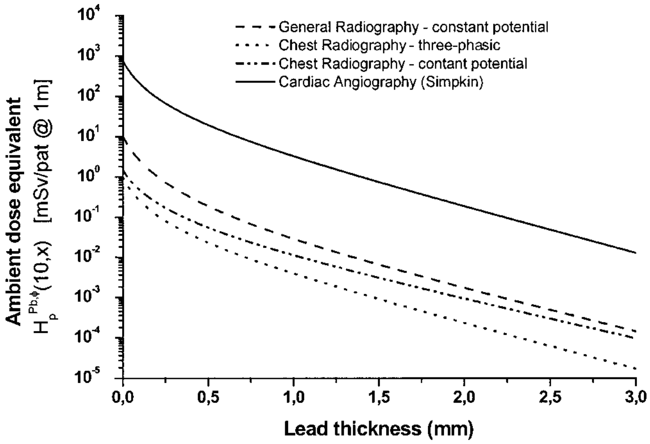

FIG. 12. Ambient dose equivalent as a function of lead thickness for primary radiation obtained applying Eq. (11) using workload spectra for general radiography (method II), chest (method II), and cardiac angiography (Simpkin—Ref. 6) techniques.

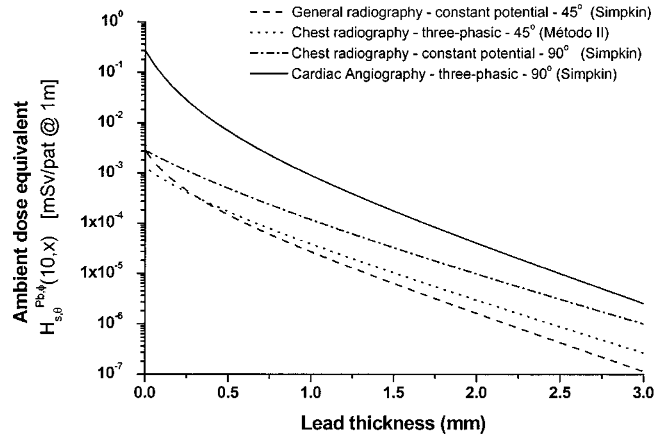

FIG. 13. Ambient dose equivalent as a function of lead thickness for secondary radiation obtained applying Eq. (21) using workload spectra for general and chest radiography considering a scattering angle of 45° and cardiac angiography technique considering a scattering angle of 90°. The considered workload spectra were obtained using method II and from Simpkin (Ref. 6).

method II, but considering also three-phasic and constant potential generators. A three-phasic generator operated following the workload evaluated by Simpkin[6] was considered for the cardiac angiography technique.

Figure 13 shows curves obtained using the same techniques and workload spectra of Fig. 12, however considering secondary radiation [Eq. (21)] in angles of 45° and 90° in relation to the primary beam. The intensity of the radiation in each case is about 10^3 smaller than the correspondent primary beams. Figure 13 also shows that the secondary radiation is composed of harder beams. This fact can be inferred by the shape of the curves (more evident for the chest technique), which appears approximately linear at the monolog scale. This behavior occurs due to the influence of the leakage component on the secondary radiation, which is heavily filtered by the housing protective materials.

Table VI shows Archer's model parameters $H_p^{0,\phi}$, α_p^m, β_p^m and γ_p^m for lead considering primary beams obtained by applying a nonlinear least-squares method.[42] The workload spectra utilized corresponds to general radiography (method II), chest (method II), and cardiac angiography (Simpkin).[6] A complete series of data corresponding to the other radiographic techniques (including mammography and computed tomography) can be obtained by contacting the authors. For each set of data the average error was evaluated and it is presented in the last column of Table VI.

Tables VII–IX show similar parameters for secondary radiation [Eq. (21)] considering the same workload spectra. The fitting process was performed for scattering angles of 10°, 45°, 90°, 135°, and 142°. In each case, the largest fitting error was 2.2%. Tables VII–IX show fitting results considering a three-phasic twelve pulse generator (3P12P) and a constant potential generator (CP).

C. Comparison with previous publications

In order to illustrate the use of the present model and to compare its results with those of previous publications,[3,11,12] two hypothetical radiological room configurations will be considered. For the primary beam model, the radiological room proposed by Dixon and Simpkin[11] will be utilized considering the shielding requirements for the floor. These authors considered a 120 patient week^{-1} room and an uncontrolled (0.02 mSv per week) fully occupied ($T=1$) area

TABLE VI. $H_p^{0,\phi}$, α_p^m, $\beta_p^m e\ \gamma_p^m$ values [Eq. (11)] for lead obtained by applying a nonlinear least-squares method for attenuation data (Ref. 42) for primary beams. The data were weighted by the workload spectra obtained in the present work (method II) and by Simpkin (Ref. 6) for general radiography, chest, and cardiac angiography techniques. $H_p^{0,\phi}$ represents the ambient dose equivalent per patient at a distance of 1 m of the focal spot (mSv/patient). For each case x-ray spectra generated by three-phasic and constant potential generators were considered. The last column shows the average error of the fitting process.

Workload spectra	X-ray generator	$H_p^{0,\phi}$ (mSv/patient at 1 m)	α_p^m (mm^{-1})	β_p^m (mm^{-1})	γ_p^m	Error (%)
General radiography	Three-phasic	6.1330	4.2134	19.2339	0.4205	2.9
(method II)	CP	7.1150	4.1557	19.2244	0.4286	2.8
Chest radiography	Three-phasic	0.9716	2.5845	17.1021	0.6318	1.4
(method II)	CP	1.0540	2.5945	16.9612	0.6277	1.4
Cardiac angiography	Three-phasic	741.8	2.6518	16.1019	0.6472	1.7
(Simpkin)	CP	799.3	2.6510	16.0166	0.6508	1.7

TABLE VII. $H_{s,\theta}^{0,\phi}$, α_s^m, $\beta_s^m e$ γ_s^m [Eq. (21)] for lead obtained by applying a nonlinear least-squares method to attenuation data (Ref. 42) for secondary beam. The data were weighted by the workload spectra obtained in the present work (method II) for general radiography technique. $H_{s,\theta}^{0,\phi}$ represents the ambient dose equivalent per patient at a distance of 1 m of the focal spot (mSv/patient). The maximum fitting error of these data was 2.2%.

Scattering angle (deg)	Archer's model parameters	X-ray generator	
		3P 12P	CP
10	$H_{s,\theta}^{0,\phi}$ (mSv/patient at 1 m)	4.47×10^{-2}	3.87×10^{-2}
	α_s^m (mm^{-1})	4.3843	4.3653
	β_s^m (mm^{-1})	9.4785	9.4636
	γ_s^m	0.3754	0.3750
45	$H_{s,\theta}^{0,\phi}$ (mSv/patient at 1 m)	3.56×10^{-5}	3.13×10^{-5}
	α_s^m (mm^{-1})	4.0485	3.9874
	β_s^m (mm^{-1})	11.4230	11.2765
	γ_s^m	0.3816	0.3918
90	$H_{s,\theta}^{0,\phi}$ (mSv/patient at 1 m)	1.61×10^{-5}	1.45×10^{-5}
	α_s^m (mm^{-1})	3.8650	3.8269
	β_s^m (mm^{-1})	12.7622	12.4062
	γ_s^m	0.3678	0.4005
135	$H_{s,\theta}^{0,\phi}$ (mSv/patient at 1 m)	5.96×10^{-2}	5.14×10^{-2}
	α_s^m (mm^{-1})	4.4443	4.3342
	β_s^m (mm^{-1})	13.0513	13.0858
	γ_s^m	0.2684	0.2660
142	$H_{s,\theta}^{0,\phi}$ (mSv/patient at 1 m)	7.28×10^{-2}	6.29×10^{-2}
	α_s^m (mm^{-1})	4.4823	4.3955
	β_s^m (mm^{-1})	12.8257	12.8735
	γ_s^m	0.2719	0.2711

distant 3.8 m from the x-ray tube focal spot. For simplicity and conservatism they also assumed $U=1$. Results from the application of these parameters by using the NCRP49 method considering two different workloads (1000 and 294 mA min week^{-1}), using Dixon and Simpkin results and the present model, are shown in Table X. For these two applications the workload spectra identified as *floor/other walls* in the Simpkin[6] and Dixon and Simpkin[11] papers were considered.

Another example was extracted from Simpkin and Dixon's paper[12] to perform this comparison for a secondary barrier. In their paper, the authors considered the workload spectra labeled *radiographic room (all barriers)*, which is a leakage technique corresponding to 150 kVp and 3.3 mA. The area to be protected was 2 m distant from the scattering medium with an angle of 90°. The beam area was $F=1000\,\mathrm{cm}^2$. Results corresponding to the application of these parameters are presented in Table XI.

In both cases the correction by using the function $(H^*(10)/k_{\mathrm{ar}})(E)$ and the constant factor (1.14) for the Gy to Sv unit conversion was considered.

IV. CONCLUSIONS

The present work provides an optimized treatment for the problem of determining shielding barriers necessary for ra-

TABLE VIII. $H_{s,\theta}^{0,\phi}$, α_s^m, $\beta_s^m e$ γ_s^m [Eq. (21)] for lead obtained by applying a nonlinear least-squares method to attenuation data (Ref. 42) for secondary beam. The data were weighted by the workload spectra obtained in the present work (method II) for chest technique. $H_{s,\theta}^{0,\phi}$ represents the ambient dose equivalent per patient at a distance of 1 m of the focal spot (mSv/patient). The maximum fitting error of these data was 2.2%.

Scattering angle (deg)	Archer's model parameters	X-ray generator	
		3P 12P	CP
10	$H_{s,\theta}^{0,\phi}$ (mSv/patient at 1 m)	3.95×10^{-3}	3.90×10^{-3}
	α_s^m (mm^{-1})	2.6853	2.6234
	β_s^m (mm^{-1})	2.9257	2.7959
	γ_s^m	0.4811	0.4422
45	$H_{s,\theta}^{0,\phi}$ (mSv/patient at 1 m)	1.50×10^{-3}	1.55×10^{-3}
	α_s^m (mm^{-1})	2.4093	2.3970
	β_s^m (mm^{-1})	3.6318	3.3884
	γ_s^m	0.6472	0.6175
90	$H_{s,\theta}^{0,\phi}$ (mSv/patient at 1 m)	1.28×10^{-3}	1.35×10^{-3}
	α_s^m (mm^{-1})	2.3701	2.3535
	β_s^m (mm^{-1})	2.9917	2.8461
	γ_s^m	0.5894	0.5574
135	$H_{s,\theta}^{0,\phi}$ (mSv/patient at 1 m)	8.44×10^{-3}	7.97×10^{-3}
	α_s^m (mm^{-1})	2.4099	2.4251
	β_s^m (mm^{-1})	10.5280	10.1767
	γ_s^m	0.5785	0.5948
142	$H_{s,\theta}^{0,\phi}$ (mSv/patient at 1 m)	9.99×10^{-3}	9.35×10^{-3}
	α_s^m (mm^{-1})	2.3563	2.3811
	β_s^m (mm^{-1})	12.0155	11.7537
	γ_s^m	0.5232	0.5454

TABLE IX. $H_{s,\theta}^{0,\phi}$, α_s^m, $\beta_s^m e$ γ_s^m [Eq. (21)] for lead obtained by applying a nonlinear least-squares method to attenuation data (Ref. 42) for secondary beam. The data were weighted by the workload spectra obtained by Simpkin (Ref. 6) for cardiac angiography technique. $H_{s,\theta}^{0,\phi}$ represents the ambient dose equivalent per patient at a distance of 1 m of the focal spot (mSv/patient). The maximum fitting error of these data was 2.2%.

Scattering angle (deg)	Archer's model parameters	X-ray generator	
		3P 12P	CP
10	$H_{s,\theta}^{0,\phi}$ (mSv/patient at 1 m)	3.40	3.17
	α_s^m (mm^{-1})	2.9880	2.9990
	β_s^m (mm^{-1})	6.0206	5.8832
	γ_s^m	0.6289	0.6327
45	$H_{s,\theta}^{0,\phi}$ (mSv/patient at 1 m)	4.78×10^{-1}	4.44×10^{-1}
	α_s^m (mm^{-1})	2.5556	2.5467
	β_s^m (mm^{-1})	9.8306	9.7790
	γ_s^m	0.5063	0.5075
90	$H_{s,\theta}^{0,\phi}$ (mSv/patient at 1 m)	2.75×10^{-1}	2.55×10^{-1}
	α_s^m (mm^{-1})	2.6027	2.5890
	β_s^m (mm^{-1})	10.7558	10.7208
	γ_s^m	0.4252	0.4276
135	$H_{s,\theta}^{0,\phi}$ (mSv/patient at 1 m)	6.88	6.88
	α_s^m (mm^{-1})	2.5889	2.5844
	β_s^m (mm^{-1})	10.7496	10.7350
	γ_s^m	0.4310	0.4298
142	$H_{s,\theta}^{0,\phi}$ (mSv/patient at 1 m)	8.72	8.10
	α_s^m (mm^{-1})	3.2617	3.2595
	β_s^m (mm^{-1})	10.9903	10.9876
	γ_s^m	0.4187	0.4200

TABLE X. Comparative results from the application of the NCRP49 method considering two different workloads (1000 and 294 mA min week^{-1}), using Dixon and Simpkin (Ref. 11) results and the present model. For these two applications the workload spectra identified as *floor/other walls* in the Simpkin (Ref. 6) and Dixon and Simpkin (Ref. 11) papers was considered. A 120 patient week^{-1} room and an uncontrolled (0.02 mSv week^{-1}) fully occupied ($T=1$) area distant 3.8 m from the x-ray tube focal spot were assumed.

	Unshielded dose (mSv week^{-1})	Lead thickness needed to reduce to 0.02 mSv week^{-1} (mm Pb)
NCRP49 $-W=1000$ mA min/wk at 120 kVcp	488.4	3.01
NCRP49 $-W=294$ mA min/wk at 120 kVcp	143.6	2.56
Dixon and Simpkin	42.8	1.45
This paper w/functional correction	76.7	2.01
This paper w/constant correction (1.14)	69.6	1.87

diological room protection. The developed method associates information regarding primary and scattered spectra usually present during diagnostic procedures as well as new data from workload spectra. This information was incorporated in a set of equations which provides the relationship between ambient dose equivalent and thickness of a shielding material considering primary, scattered, and leakage radiation from a given diagnostic procedure. The equations can generate families of attenuation curves, which are very useful during diagnostic rooms shielding design.

The developed set of equations is based on previous models for primary[11] and secondary[12] radiation, but it takes into account the radiation spectra modulated by the workload distribution. This formulation was chosen because of its ability to compensate the variation of the spectral shape when the radiation beam crosses the shielded wall. Figure 14 shows the radiation spectra calculated using Eq. (10) without performing the integration on the variable E. The curves were calculated using primary beams modulated by the workload spectra from Simpkin[6] for general radiography considering the incident radiation and the radiation transmitted by 0.5 mm Pb. The attenuation by the patient was not considered nor the construction materials of the wall. They represent approximate spectra that could be measured by solid-state detectors placed in the primary beam, inside and outside a diagnostic room, divided by the number of patients imaged during the integration period. As lead was used as shielding material, the 88 keV k-edge is very evident in the transmitted spectra. In spite of the approximations, this extended model provides a most accurate approach for determining shielding barriers for diagnostic installations.

The model can be improved when associated with the most complete data regarding the attenuation properties of shielding and constructing materials,[5,43] and the attenuation of the patient and devices used for performing diagnostic imaging.[10] Moreover, the scattered spectra used in the present work were obtained just for constant potential generators and do not include information for the mammography technique. Complementary work is in progress in order to provide this additional information.

For a typical primary beam, Table X shows an estimation of the unshielded radiation as 1.8 times [with functional conversion by using the function $(H^*(10)/k_{ar})(E)$] and 1.6 times (by using a constant conversion of 1.14) the value obtained by Dixon and Simpkin.[11] This result likely reflects the differences on output value of the x-ray equipment considered in each case. Dixon and Simpkin determined an unshielded primary dose at 1 m from the focal spot as 5.15 mGy patient^{-1}, while the result by integration of the spectral distribution of the radiation (considering the same workload spectra) was 7.35 mGy patient^{-1}. Moreover, the unit conversion used by these authors was 1 mGy=1 mSv and the functional correction factor used in the present work increases this value by about 15%.

TABLE XI. Comparative results for secondary barrier from the application of NCRP49 method considering two workloads (1000 and 294 mA min wk^{-1}), using Simpkin and Dixon (Ref. 12) results and the present model. For these two applications the workload spectra labeled *radiographic room (all barriers)* and a leakage technique corresponding to 150 kVp and 3.3 mA were considered. The area to be protected was 2 m distant to the scattering medium, with an angle of 90°. The beam area was $F=100$ cm^2. For the present model, the correction by using the function $(H^*(10)/k_{ar})(E)$ and also a constant factor (1.14) to Gy to Sv unit conversion were considered.

	Unshielded dose (mSv week^{-1})	Lead thickness needed to reduce to 0.02 mSv week^{-1} (mm Pb)
NCRP49 $-W=1000$ mA min/wk at 120 kVcp	15.0	1.93
NCRP49 $-W=294$ mA min/wk at 120 kVcp	4.4	1.49
Simpkin and Dixon	1.03	0.6
This paper w/functional correction	0.10	0.22
This paper w/constant correction (1.14)	0.08	0.19

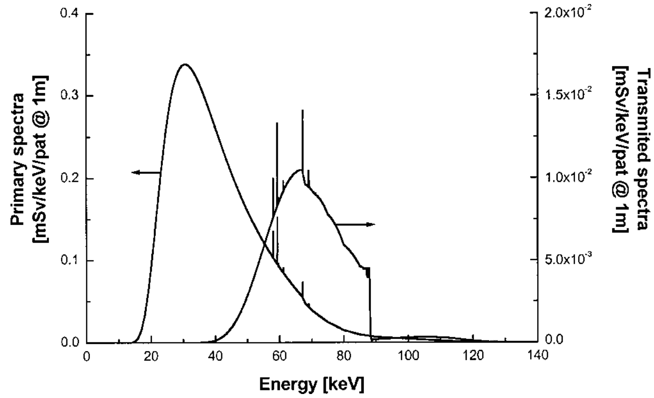

FIG. 14. Primary spectra incident and transmitted through 0.5 mm Pb, considering a typical diagnostic installation (Simpkin—Ref. 6), performing general radiographic techniques.

For the secondary beam, Table XI shows that the estimation for the unshielded dose was around ten times lower than the values obtained by Simpkin and Dixon.[12] Our calculations resulted in 1.20×10^{-3} mSv/mA min at 1 m for the unshielded leakage radiation and 2.29×10^{-3} mSv/mA min at 1 m for the unshielded scatter radiation (total 3.49×10^{-3} mSv/mA min at 1 m), against 5.32×10^{-4} mSv/mA min at 1 m and 3.37×10^{-2} mSv/mA min at 1 m (total 3.42×10^{-2} mSv/mA min at 1 m) for the same unshielded leakage and scatter radiation obtained by Simpkin and Dixon. This discrepancy probably was determined for three reasons: (i) the field size used by Fehrenbacher *et al.*[30] was smaller than the phantom size and, therefore, part of the scattered radiation was attenuated during its path inside the phantom; (ii) the magnitude of $N_e^{\phi,V}(E,\theta)$ was inferred from output data used in Fehrenbacher's experiments. This magnitude is just a crude approximation of the real value which must be used for the correct evaluation of Eqs. (13) and (14); (iii) the calculation of the unshielded scatter radiation [Eq. (14) considering $x_e=0$] takes into account the use of Eq. (13), which can only be correctly used when the scattered spectra is generated by its correspondent primary spectra. A more accurate calculation was not done because this kind of data was not found in the literature. The authors believe that a more precise calculation of these spectra can reduce these differences. Anyway, the presented calculation was introduced in this work just to exemplify the use of the presented model and must not be used as a numerical reference.

Comparative results[44] of the application of the NCRP49 method and the formulation presented in this work in two real imaging diagnostic departments show a cost reduction of around 50% when using this optimized process. This value was obtained considering barrier calculations of two real situations performed by using the proposed method and applying a computer program designed by Simpkin.[45] The reduction in costs was estimated by considering the amount of lead necessary to shield these two imaging departments in each case. On average, the proposed methodology implies in using half of the lead thickness necessary to correctly shield these areas, when compared with the necessary thickness obtained by applying the NCRP49 method. This result demonstrates that the development of an optimized methodology for shielding calculation in diagnostic rooms can be associated with a cost-benefit analysis to be performed during the design process of a radiological department.

ACKNOWLEDGMENTS

The authors gratefully acknowledge the contributions of Dr. Sílvio B. Herdade, Dr. Ricardo A. Terini, and Márcia C. Silva during several parts of this work. Thanks are also due to Denise Y. Nersissian, Tânia A. C. Furquim, and Marco A. G. Pereira for helpful discussions and suggestions during the development of the generalized model. Very special thanks are due to Dr. Thomas Fewell, from CDRH/FDA, who kindly provided some of the spectral data used in this work, and to Dr. Benjamin Archer, who provided the program for the nonlinear least-squares fitting. This work was supported by Fundação de Amparo à Pesquisa do Estado de São Paulo and Conselho Nacional de Desenvolvimento Científico e Tecnológico, Brazil.

[a]Electronic mail: pcosta@iee.usp.br
[b]Electronic mail: lcaldas@net.ipen.br
[1] B. R. Archer, "History of the shielding of diagnostic x-ray facilities," Health Phys. **69**, 750–758 (1995).
[2] National Council on Radiation Protection and Measurements, "Medical X-ray protection up to two million volts," Report No. 6, NCRP, Bethesda, MD, 1949.
[3] National Council on Radiation Protection and Measurements, "Structural shielding design and evaluation for medical use of x rays and gamma rays of energies up to 10 MeV," Report No. 49, NCRP, Bethesda, MD, 1976.
[4] B. R. Archer, J. I. Thornby, and S. C. Bushong, "Diagnostic x-ray shielding design based on an empirical model of photon attenuation," Health Phys. **44**, 507–517 (1983).
[5] B. R. Archer, T. R. Fewell, B. J. Conway, and P. W. Quinn, "Attenuation properties of diagnostic x-ray shielding materials," Med. Phys. **21**, 1499–1507 (1994).
[6] D. Simpkin, "Evaluation of NCRP Report No. 49 assumptions on workloads and use factors in diagnostic radiology facilities," Med. Phys. **23**, 577–584 (1996).
[7] O. H. Suleiman, B. J. Conway, T. R. Fewell, R. J. Slayton, and F. G. Rueter, "Radiation protection requirements for medical x-ray film," Med. Phys. **22**, 1691–1693 (1995).
[8] B. R. Archer, "Diagnostic x-ray shielding design—new data and concepts," in *The Expanding Role in Medical Physics in Diagnostic Imaging*, edited by D. Frey and P. Spraws, Proceedings of the 1997 AAPM Summer School (Advanced Medical Publishing, Madison, WI, 1997).
[9] R. L. Dixon and D. J. Simpkin, "New concepts for radiation shielding of medical diagnostic x-ray facilities," in Ref. 8.
[10] R. Dixon, "On the primary barrier in diagnostic x-ray shielding," Med. Phys. **21**, 1785–1793 (1994).
[11] R. L. Dixon and D. J. Simpkin, "Primary shielding barriers for diagnostic x-ray facilities: A new model," Health Phys. **74**, 181–189 (1998).
[12] D. J. Simpkin and R. L. Dixon, "Secondary shielding barriers for diagnostic x-ray facilities: Scatter and leakage revisited," Health Phys. **74**, 350–365 (1998).
[13] D. J. Simpkin, "Transmission data for shielding diagnostic x-ray facilities," Health Phys. **68**, 704–709 (1995).
[14] D. J. Simpkin, "Shielding a spectrum of workloads in diagnostic radiology," Health Phys. **61**, 259–261 (1991).
[15] D. M. Tucker, G. T. Barnes, and D. P. Chakraborty, "Semiempirical model for generating tungsten target x-ray spectra," Med. Phys. **18**, 211–218 (1991).
[16] R. Birch and M. Marshall, "Computation of bremsstrahlung x-ray spectra and comparison with spectra measured with a Ge(Li) detector," Phys. Med. Biol. **24**, 505–517 (1979).

[17] H. M. Kramer, H.-J. Selbach, and W. J. Iles, ‘‘The practical peak voltage of diagnostic x-ray generators,’’ Br. J. Radiol. **71**, 200–209 (1998).
[18] H. E. Johns and J. R. Cunninghan, *The Physics of Radiology*, 4th ed. (Thomas, Springfield, 1983).
[19] D. M. Tucker, G. T. Barnes, and X. Wu, ‘‘Molybdenum target x-ray spectra: A semiempirical model,’’ Med. Phys. **18**, 402–407 (1991).
[20] A. B. Wolbarst, *Physics of Radiology* (Appleton & Lange, Norwalk, 1993).
[21] R. A. Terini, P. R. Costa, T. A. C. Furquim, and S. B. Herdade, ‘‘Measurements of discrete and continuous x-ray spectra with a photodiode at room temperature,’’ Appl. Radiat. Isot. **50**, 343–353 (1999).
[22] T. R. Fewell (personal communication).
[23] International Electrotechnical Commission, ‘‘*Medical diagnostic x-ray equipment—Radiation condition for use in the determination of characteristics*,’’ Publ. No. 1267, Genève, 1994.
[24] J. M. Crickenberger, *Calibration Laboratories Technical Guide* (NIST, Washington, DC, 1995).
[25] M. Carvalho, S. B. Herdade, P. Lammoglia, P. R. Costa, and R. A. Terini, ‘‘Determination of the voltage applied to x-ray tubes from the bremsstrahlung spectrum obtained with a silicon PIN photodiode,’’ Med. Phys. **27**, 2617–2623 (2000).
[26] B. R. Archer, T. R. Fewell, B. J. Conway, P. W. Quinn, R. E. Shupping, and S. P. McBridge, *Photon Attenuation Properties of Diagnostic X-ray Shielding Materials* (CDRH, FDA, 1990).
[27] E. Trout and J. P. Kelley, ‘‘Scattered radiation from a tissue equivalent phantom for x-rays from 50 to 300 kVp,’’ Radiology **104**, 161–169 (1972).
[28] C.-W. Cheng, K. W. Taylor, and A. F. Holloway, ‘‘The spectrum and angular distribution of x-rays scattered from a water phantom,’’ Med. Phys. **22**, 1235–1245 (1995).
[29] N. W. Marshall, K. Faulner, and H. Warren, ‘‘Measured scattered x-ray energy spectra for simulated irradiation geometries in diagnostic radiology,’’ Med. Phys. **23**, 1271–1276 (1996).
[30] G. Fehrenbacher, W. Panzer, and K. Tesfu, ‘‘*Spectra of Diagnostic X-rays Scattered by a Water Phantom. Institut für Strahlenshutz*,’’ GSF Publ. No. 9/96, Neuherberg, 1996.
[31] G. Fehrenbacher, K. G. Tesfu, W. Panzer, and D. Regulla, ‘‘Determination of diagnostic x ray spectra scattered by a phantom,’’ Radiat. Prot. Dosim. **71**, 305–308 (1997).
[32] D. J. Simpkin, ‘‘Scatter radiation intensities about mammography units,’’ Health Phys. **70**, 238–244 (1996).
[33] P. R. Costa and L. V. E. Caldas, ‘‘Diagnostic x-ray room design using photon attenuation and spectrum evaluation models: Simulation and partial results,’’ in World Congress of Medical Physics and Biomedical Engineering, 14–19 September 1997, Nice Med. Biol. Eng. Comput. **33,** 1162 1997.
[34] P. R. Costa, ‘‘Model for determination of protective shielding needed for diagnostic radiology rooms,’’ Ph.D. thesis abstracts, Med. Phys. **27**, 1698 (2000).
[35] P. R. Costa and L. V. E. Caldas, ‘‘Model for determination of protective shielding thickness for diagnostic radiology rooms,’’ Proceedings of the International Radiation Protection Association, Hiroshima–Japan, 14–19 May 2000.
[36] P. R. Costa and L. V. E. Caldas, ‘‘Evaluation of protective shielding thickness for diagnostic radiology rooms,’’ oral presentation at the student paper competition of World Congress of Medical Physics and Biomedical Engineering, Chicago, 24–27 July 2000.
[37] International Commission on Radiological Units and Measurements, ‘‘Conversion coefficients for use in radiological protection against external radiation,’’ ICRU Report No. 57, Bethesda, MD, 1998.
[38] International Commission on Radiological Units and Measurements, ‘‘Measurement of dose equivalents from external photon and electron radiations,’’ ICRU Report No. 47, Bethesda, MD, 1992.
[39] E. Trout and J. P. Kelley, ‘‘Scattered radiation from a tissue equivalent phantom for x-rays from 50 to 300 kVp,’’ Radiology **104**, 161–169 (1972).
[40] International Electrotechnical Commission, ‘‘*Medical electrical equipment. 1. General requirements for safety. 3. Collateral standard: General requirements for radiation protection in diagnostic x-ray equipment*,’’ IEC Publ. No. 60601.1.3. Genève, 1994.
[41] J. E. Peixoto, ‘‘*Determinação dos fatores de atenuação e dos coeficientes de conversão em termos do equivalente de dose ambiental e da dose efetiva para raios X gerados na faixa de 50 a 150 kVp*,’’ Rio de Janeiro, 1994; Ph.D. thesis, Centro de Ciências da Saúde, Universidade Federal do Rio de Janeiro (in Portuguese).
[42] B. Archer, Program LNKUXFIT (personal communication).
[43] S. F. Barros, H. R. Schelin, P. R. Costa, J. Tilly, M. A. G. Pereira, C. Gomes, S. B. Herdade, M. C. Silva, and R. A. Terini, ‘‘Evaluation of attenuation properties of some common and special building materials,’’ Proceedings of the World Congress of Medical Physics and Biomedical Engineering, Chicago, 24–27 July 2000.
[44] P. R. Costa, ‘‘*Modelo para determinação de espessuras de barreiras protetoras para salas de radiologia diagnóstica*,’’ Ph.D. thesis, Universidade de São Paulo, 2000 (in Portuguese).
[45] D. J. Simpkin, Kux: X-ray shielding specifications. Computer program, 1990.